

# Constraints on Common Envelope Magnetic Fields from Observations of Jets in Planetary Nebulae

James Tocknell, Orsola De Marco, Mark Wardle

*Department of Physics and Astronomy, Macquarie University, Sydney, NSW 2109, Australia*

*Astronomy, Astrophysics and Astrophotonics Research Centre, Macquarie University, Sydney, NSW 2109, Australia*

9 January 2020

## ABSTRACT

The common envelope (CE) interaction describes the swallowing of a nearby companion by a growing, evolving star. CEs that take place during the asymptotic giant branch phase of the primary may lead to the formation of a planetary nebula (PN) with a post-CE close binary in the middle. We have used published observations of masses and kinematics of jets in four post-CE PN to infer physical characteristics of the CE interaction. In three of the four systems studied, Abell 63, ETHOS 1 and the Necklace PN, the kinematics indicate that the jets were launched a few thousand years before the CE and we favour a scenario where this happened before Roche lobe overflow, although better models of wind accretion and wind Roche lobe overflow are needed. The magnetic fields inferred to launch pre-CE jets are of the order of a few Gauss. In the fourth case, NGC 6778, the kinematics indicate that the jets were launched about 3000 years *after* the CE interaction. Magnetic fields of the order of a few hundreds to a few thousands Gauss are inferred in this case, approximately in line with predictions of post-CE magnetic fields. However, we remark that in the case of this system, we have not been able to find a reasonable scenario for the formation of the two jet pairs observed: the small orbital separation may preclude the formation of even one accretion disk able to supply the necessary accretion rate to cause the observed jets.

**Key words:** Magnetic Fields, ISM: Jets and Outflows, Planetary Nebulae: Individual: Necklace, Planetary Nebulae: Individual: Abell 63, Planetary Nebulae: Individual: ETHOS 1, Planetary Nebulae: Individual: NGC 6778

## 1 INTRODUCTION

A common envelope (CE) interaction between a giant and a more compact companion happens when the envelope of the primary giant star grows sufficiently large as to engulf the secondary. The orbital energy unbinds the envelope, leaving either a close binary composed of a white dwarf (the core of the giant) and the companion or, if the secondary lacks sufficient energy to unbind the envelope, a merger (Paczynski 1976; Ivanova et al. 2013).

The shapes of most planetary nebulae (PN) diverge significantly from spherical (Parker et al. 2006). The reason may be that a companion has played a role during the mass-losing asymptotic giant branch (AGB) phase during which the PN gas was ejected (Soker 1997; De Marco et al. 2009). While for most PN with non-spherical shapes we presume the action of a companion, for approximately one in five PN *we know* that a companion has ejected the envelope (Bond 2000; Miszalski et al. 2009). Common envelope PN are identified by the presence of a close binary in the centre of a PN. On occasion a PN surrounding a post-CE central binary turns out to be a Stroemgren sphere around a post-red giant branch star, rather than a proper PN (Frew & Parker 2010; e.g., EGB 5; Geier et al. 2011). PN around post-CE binaries are not only

interesting because they are cases for which we know the mechanisms that imparted the PN its shape (e.g. Miszalski et al. 2009), but also because they provide a unique tool for the study of the CE interaction. In post-CE PN the existence and brightness of the PN guarantees that the CE interaction only took place a few thousand years ago at most. Also, the aftermath of the ejection is there to be studied.

In this paper we focus on four PN around post-CE binaries, which exhibit jet-like structures. These have been measured and their kinematics indicate that three of the four objects launched their jets before the main nebula, a clear indication that an accretion disk formed before the companion plunged into the primary. In the fourth case not one, but two pairs of jets are observed. Both these jet pairs are kinematically younger than the nebula, demonstrating that they were launched after the CE interaction had taken place.

We assume here that all CE jets are launched via an accretion disk threaded by a magnetic field (Blandford & Payne 1982). The launch efficiency, or the fraction of accreted mass that is ejected, is between 10% and 50% in this model (Sheikhnezami et al. 2012). We also assume that the magnetic field responsible for the jet launching and collimation is also responsible for the loss of angular momentum and accretion of disk material (Wardle 2007). Within

this model, we use the jet properties to determine the magnetic field responsible for the mass accretion and jet launching in pre and post-CE phases.

In section §2 we review the four PN which will be analysed in this paper, outlining the kinematics and morphology of these objects. Section §3 contains our examination of a number of different scenarios for launching the jets. In Section §4 we discuss the magnetic fields that are implied for the four PN under the assumptions of our models and compare them, in the case of the post-CE PN, to the magnetic fields theoretically derived in a model by Regos & Tout (1995). In Section §5, we discuss scenarios for the formation of the post-CE jets of NGC 6778 and in Section §6 we briefly discuss two additional post-CE PN. Finally, in Section §7, we summarise and conclude.

## 2 POST-CE SYSTEMS WITH JETS

A few PNe with jets are known to contain post-CE central star binaries, but in only four cases have we sufficient information to carry out our study: the Necklace (PN G054.2–03.4; Corradi et al. 2011), Abell 63 (PN G053.8–03.0, whose central stars is known as UU Sagittae; Mitchell et al. 2007; Afşar & Ibanoglu 2008), ETHOS 1 (PN G068.1+11.0; Miszalski et al. 2011a) and NGC 6778 (PN G034.5–06.7; Guerrero & Miranda 2012; Miszalski et al. 2011b). In order to develop a model for launching the observed jets, we need values for the kinematic parameters and masses of the circumstellar material. These are summarised in Table 1.

### 2.1 The Necklace

The Necklace PN (PN G054.2–03.4; Fig. 1, left panel) consists of a ring with radius  $6.5 \pm 0.5$  arcsec expanding at  $28 \pm 3$  km s<sup>-1</sup> on a plane inclined by  $59 \pm 3^\circ$  to the line of sight, where  $0^\circ$  is in the plane of the sky (Corradi et al. 2011). Two polar caps are assumed to be perpendicular to the plane of the ring. The northern cap is quite compact and spans a distance of 38 to 46 arcsec from the star. The southern cap is more extended and spans a distance of 37 to 59 arcsec (measured by us on figure 4 of Corradi et al. (2011)). All the gas in each cap appears to move with the same velocity: de-projected velocities are 95 and 115 km s<sup>-1</sup>, for the northern and southern caps, respectively. We gauged the errors on these velocities to be 3 km s<sup>-1</sup> from figure 4 of Corradi et al. (2011). The kinematic ages are determined by dividing the ring radius (or the deprojected distance between the star and the base or tip of each jet cap) by the de-projected ring expansion velocity (or de-projected velocity of the caps). For the ring, Corradi et al. (2011) find a kinematic age of 1100 yr kpc<sup>-1</sup>. The error on this estimate can be estimated to be 25%. The kinematic age of the innermost part of the southern cap is 1900 yr kpc<sup>-1</sup>, while for the outermost part it is 2800 yr kpc<sup>-1</sup>. The northern cap has an average age of 2500 yr kpc<sup>-1</sup>. The error on these estimates can be determined to be 20%. The lack of a velocity gradient along the caps implies that material was ejected during a certain period of time, as opposed to during a quick outburst. The distance to this PN was kindly measured by D. Frew to be  $4.6 \pm 1.1$  kpc by applying the surface brightness-radius relation (Frew 2008). At that distance the ring has an age of  $\sim 5000$  years while the age of the polar caps would be in the range 8700–13 000 years. Using this distance estimate, the time over which the jet was launched is  $\sim 4000 - 8000$  yr, which agrees with the assertion that the ejection was not a quick outburst.

The ionised mass of the entire nebula was estimated from the integrated  $H_\alpha$  flux and a filling factor of 0.4 to be  $0.06 \pm 0.03 M_\odot$ . The ionised mass of the caps is of the order of  $10^{-3} M_\odot$  (R. Corradi, private communication). These mass estimates as well as the estimates of the kinematic ages determined above, will suffer from an additional source of uncertainty, which is hard to quantify, but which we argue to be smaller than an order of magnitude. All ejected material impacts the circumstellar ambient medium. This will potentially increase the mass of the ejected structures and decrease their speeds over time.

We argue here that it is unlikely that the PN body and jets have slowed down dramatically. The velocities measured along the cap (particularly the southern cap which spans a range of about 20 arcsec) are surprisingly constant with no real indication that the material launched most recently is significantly faster (if anything the gas closest to the star is slowest). We also present circumstantial evidence that the measured velocities are not much smaller than the ejection velocities, and in any case not by more than a factor of a two: the jet velocities measured for the PN A63 (Section §2.2), ETHOS 1 (Section §2.3) and FLEMING 1 (Section §6) are all approximately 100 km s<sup>-1</sup>, something that would be unlikely were they slowed down considerably by material in four different circumstellar environments.

The momentum conservation considerations presented by Blackman (2009) could be applied in the current case to estimate the amount of mass loading and the velocity decrease. However, contrary to the case described by Blackman (2009), where the *pre*-PN jets are punching through the entire AGB star envelope (which has just been ejected in the superwind phase), the present case is different. The common envelope is likely to take place before the super wind ensues. We argue this on probabilistic grounds. The chance that the capture of a companion coincides with the very short, final, phase of the AGB star life is unlikely. It is more likely that at some point in the upper AGB, but before the superwind phase, the companion was captured. In such case the circumstellar material encountered by the jet would be far less dense than in the case of a jet perforating the super wind-formed shell, which is effectively the entire AGB envelope. Even wanting to follow through with the calculation of Blackman (2009), the uncertainty in determining the swept up mass would outweigh that of assuming that the jet mass today is the same as the ejected mass, which, we argued above, should only be within a factor of less than two.

Finally, we note that for the central star of the Neckalce PN, there is independent observational evidence that accretion has occurred onto the companion (Miszalski et al. 2013), because of the pronounced carbon abundance of this otherwise normal main sequence star. The estimated amount of accreted matter was  $0.03 - 0.35 M_\odot$  for a  $1.0 - 0.4 M_\odot$  companion. Inspection of the equations used by Miszalski et al. (2013), reveals that in the case of a  $0.3 M_\odot$  main sequence companion, which is almost fully convective, we expect between  $0.10$  and  $0.42 M_\odot$  of gas accreted to raise the C/O ratio to unity from the solar value, for a range of AGB C/O ratios of  $1.5 - 3$ . In Section §3.2 we will consider whether such a large accreted mass is in line with the deduced accretion rates and jet mass-loss rates.

### 2.2 Abell 63

Abell 63 (PN G053.8–03.0) is a faint planetary nebula discovered by Abell (1966), with the binarity of central star discovered by Bond et al. (1978). Like the Necklace, it appears as an edge-on ring with two caps. Mitchell et al. (2007) provided detailed kinematic

**Table 1.** Properties of the common envelope PN in our sample

Object	The Necklace	Abell 63	ETHOS 1	NGC 6778
Deprojected expansion velocity of main nebula/ring ( $\text{km s}^{-1}$ )	$28 \pm 3$	$\sim 26$	$\sim 55$	$\sim 26$
Deprojected velocity of jets ( $\text{km s}^{-1}$ )	95(N), 115(S) <sup>a</sup>	$126 \pm 23^a$	$120 \pm 10^d$	$270^e; 460^f$
Ionised gas mass of nebula/ring ( $M_\odot$ )	$0.06 \pm 0.03$	0.09	–	–
Ionised gas mass of jets ( $M_\odot$ )	$\sim 10^{-3}$	–	–	$\sim 1.5 \times 10^{-3g}$
Radius of nebula/ring (arcsec)	$6.5 \pm 0.5$	$\sim 14$	$\sim 9.7$	$\sim 8.5$
Distance to jet tips from star (arcsec)	$\sim 60$	$\sim 142$	$\sim 31.3$	$\sim 35$
Age of nebula/ring (yr)	$\sim 5000$	$\sim 11200$	$\sim 5400$	$\sim 4400$
Age of jets (yr)	$\sim 8700^b - 13000^c$	$\sim 17100$	$\sim 10500$	$\sim 1700$
Jet ejection timescale (yr)	3700 – 8000	5900	5100	1700
Jet mass-loss rate ( $M_\odot \text{ yr}^{-1}$ )	$1 - 3 \times 10^{-7}$	–	–	$8.8 \times 10^{-7}$
Period of central binary (days)	1.2	0.46	0.53	0.15
Distance to object (kpc)	$4.6 \pm 1.1$	$3.2 \pm 0.6$	$6.0^{+2.5}_{-1.5}$	$2.6^{+0.7}_{-0.8}$

<sup>a</sup> Average velocity of caps.

<sup>b</sup> Edge of southern cap closest to central star.

<sup>c</sup> Edge of southern cap furthest from central star.

<sup>d</sup> Velocity of jet tips.

<sup>e</sup> Linear jet.

<sup>f</sup> Curved jet.

<sup>g</sup> Mass of each pair.

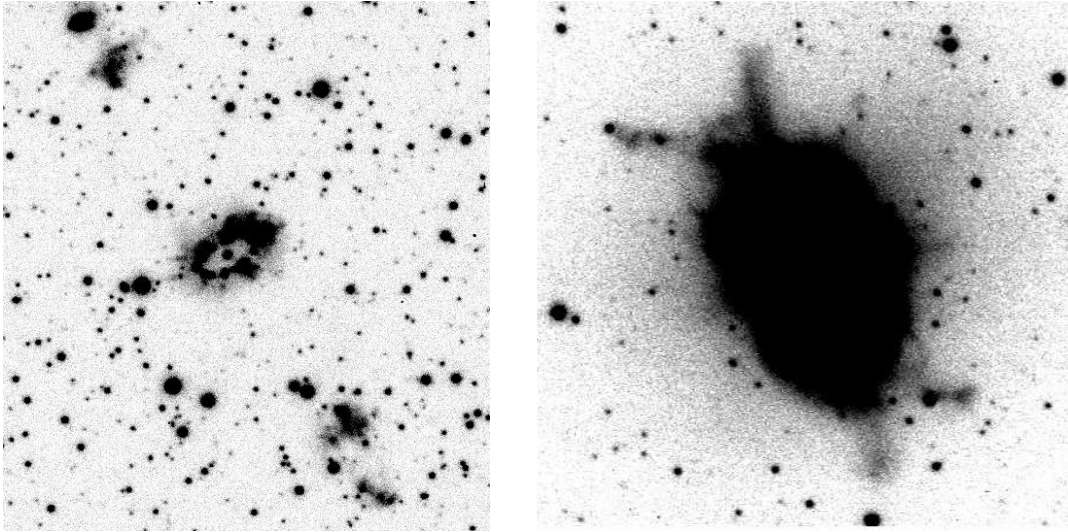


**Figure 1.** Left panel: An [NII] image of the Necklace PN created using data from Corradi et al. (2011). The height of the image is approximately 100 arcsec. Right panel: an  $H_\beta$  image of NGC 6778 adapted using data from Guerrero & Miranda (2012). The image’s height is approximately 70 arc seconds. In both images, North is to the top and East is to the left. Both images were scaled so as to emphasise the jet structures. For additional PN structure details refer to the original papers

and morphological measurements of the PN. The inclination of the system was determined to be  $87.5^\circ$  (where  $0^\circ$  is in the plane of the sky), assuming that the inclination of the system is the same as the inclination of the binary.

Mitchell et al. (2007) measured the expansion velocity of the ring or torus structure to be  $\sim 26 \text{ km s}^{-1}$ . The average radial velocities of the caps are  $5.5 \pm 1 \text{ km s}^{-1}$ , and when the inclination of the system is taken into account, the average velocities of the caps are  $126 \pm 23 \text{ km s}^{-1}$ . Frew (2008) measured the ionised mass of Abell 63 to be  $0.09 M_\odot$ , using a filling factor of 0.4, similar to the total PN mass of the Necklace nebula. No jet mass estimate exists for this object. Mitchell et al. (2007) derived kinematic ages of the structures using a distance of 2.4 kpc, which they attributed to Pollacco & Bell (1993). However, those authors actually

derived a distance of  $3.2 \pm 0.6$  kpc from the eclipsing binary system, a directly-determined distance which we use in the present study. The surface brightness-radius relation of Frew (2008) results in a smaller distance estimate of  $2.6^{+1.0}_{-0.5}$  kpc which is consistent with the eclipsing binary distance estimate within the large error bars. We have rescaled the dynamical ages of the nebular structures of Abell 63 to the distance of 3.2 kpc:  $\sim 11\,200$  yr for the ring and  $\sim 17\,100$  yr for the jets. These larger age values are in line with the appearance of Abell 63, characteristic of an old nebula. According to these figures, the jet predates the nebula by  $\sim 5900$  yr. We gauge the errors on these estimates to be similar to those estimated for the Necklace PN case (Section §2.1). Finally, Mitchell et al. (2007) suggests that the ejection was fairly rapid, contrary to the case of the Necklace PN, because the morphology of the jets of Abell 63

match those of Mz 3, which is known to have had launched the jets over a short amount of time.

### 2.3 ETHOS 1

ETHOS 1 (PN G068.1+11.0) was discovered by Miszalski et al. (2011a), as part of a survey of the SuperCOSMOS Science Archive (Hambly et al. 2004). This nebula appears as a torus, with two perpendicular outflows. The angle of inclination of the disk was given as  $60 \pm 5^\circ$  to the line of sight, where  $0^\circ$  is in the plane of the sky. The torus has radius of  $\sim 10$  arcsec and a radial velocity gradient with a maximum velocity of  $55 \text{ km s}^{-1}$ , possibly implying a short timescale for the ejection. The SE jet has radial velocity  $-55 \pm 5 \text{ km s}^{-1}$  and the NW jet has radial velocity  $65 \pm 5 \text{ km s}^{-1}$ . The de-projected velocities of the jets are  $120 \pm 10 \text{ km s}^{-1}$  (Miszalski et al. 2011a), assuming that the jets are symmetric. Miszalski et al. (2011a) give kinematic age calculations for both the jets,  $1750 \pm 250 \text{ yr kpc}^{-1}$ , and for the inner nebula  $900 \pm 100 \text{ yr kpc}^{-1}$ . There are no distance estimates for ETHOS 1 in the literature. Using the surface brightness-radius relation, a distance of  $6.0^{+2.5}_{-1.5} \text{ kpc}$  can be derived (Frew 2008). With this distance the age of the jets is 10 500 yr, and the age of the ring is 5400 yr, implying that the jets predate the nebula by  $\sim 5100$  yr. We estimate the errors on these estimates to be similar to those estimated for the Necklace PN case (Section §2.1). No mass estimates exist for this PN.

### 2.4 NGC 6778

The PN NGC 6778 (PN G034.5–06.7; Fig. 1, right panel) was discovered to harbour a post-CE central star by Miszalski et al. (2011b). Maestro et al. (2004) and Guerrero & Miranda (2012) carried out detailed kinematical analysis of the nebula. The equatorial ring has a radius of 8.5 arcsec. The ring has an inclination to the line of sight of  $\sim 75 - 78^\circ$  (where  $0^\circ$  is in the plane of the sky) and was observed to expand with a de-projected velocity of  $26 \text{ km s}^{-1}$ . From the ring protrude two lobes extending approximately 20 arcsec from the centre of the nebula. The de-projected expansion velocity at the tip of the lobes is  $50 \text{ km s}^{-1}$ . The authors note that the lobes lack a typical velocity structure, and suffer instead from great complexity, as if they had been bored along selected directions.

The agent responsible for the shaping seems to be two pairs of collimated features extending farther than the lobes, to  $\sim 35$  arcsec from the centre of the nebula. One pair is linear and is approximately aligned with the bipolar lobes. The second pair starts near the star with the same inclination but curves at the tips with point symmetry. Both pairs of jets exhibit a velocity gradient, with velocity increasing as the distance from the centre. Assuming the normal to the disk plane makes an angle of  $78^\circ$  with the line of sight, the jets have deprojected velocities of  $270 \text{ km s}^{-1}$ , for the linear jets and  $460 \text{ km s}^{-1}$ , for the curved jets. The kinematic ages of the ring and lobes are  $1700 \text{ yr kpc}^{-1}$  and  $1600 \text{ yr kpc}^{-1}$ , respectively, while for the linear jets it is  $650 \text{ yr kpc}^{-1}$ . *This clearly indicates that the jets of NGC 6778 were launched after the main nebula, contrary to those of the other three post-CE PN analysed here.* This is one of two post-CE PN for which the jets are kinematically younger than the main nebula (the other, NGC 6337, is described in Section §6).

The lack of any change in the images taken three years apart imposes a lower limit on the distance of 1 kpc. The 9 distance

estimates listed in the ESO PN catalogue (Acker 1992) range between 1.9 and 3.1 kpc, with only one estimate at 8.1 kpc. The surface brightness-radius distance to this object is  $2.6^{+0.7}_{-0.8} \text{ kpc}$  (Frew 2008). Using this distance estimate we calculate that the jets are 1700 years old, while the main nebula is 4400 years old. In this nebula the jets lag the nebular ejection by 2700 yr.

The mass of the jets was kindly obtained by M. Guerrero. The average  $H_\beta$  surface brightness in the jets is  $\sim 1.0 \times 10^{-16} \text{ erg cm}^{-2} \text{ s}^{-1} \text{ arcsec}^{-2}$ , with an uncertainty of 15% to account for the spectroscopic calibration and extinction correction uncertainties, and for the slit location on the nebula. Then, assuming the jets to be “cylinders” of radius 2 arcsec and height 27 arcsec for the linear jets and 23 arcsec for the curved jets a root mean square density  $N_e \sim 110 \times \epsilon^{-0.5} \text{ cm}^{-3}$  is obtained. This leads to masses of  $1.2 \times 10^{-4} \epsilon^{0.5} D^{2.5} M_\odot$  for each linear jet, and  $9.9 \times 10^{-5} \epsilon^{0.5} D^{2.5} M_\odot$  for each curved jet, where  $D$  is the distance to the object in kiloparsecs and  $\epsilon$  is the filling factor. If we adopt a filling factor of 0.4 and a distance of 2.6 kpc, we obtain jet masses of  $1.6 \times 10^{-3} M_\odot$  and  $1.4 \times 10^{-3} M_\odot$  for the linear and curved jet *pairs*, respectively.

The formal error in the determination of the ring radius and location of the caps from the spatio-kinematic analysis is approximately 2 arcsec, while the velocity error is due to the width of the line and can be (generously) determined to be  $10 \text{ km s}^{-1}$ . The error in the inclination is approximately 3 deg. So the formal error on the distance-independent ages is approximately 40%. Applying this error in opposite directions to the kinematic age of the jets and the ring, so as to reduce their difference, brings the two values to be within 100 yrs of one another. Although this would effectively indicate coevality of the structure, it is unlikely that the sequence of the ejection would be completely reversed (jets before nebula as is the case for the three PN described above). As we will point out later on, these jets have many differences to the ones just described but do have commonalities with another object, NGC 6337, which we describe in Section §6.

Another concern is that the slit that measured the curved jet did not overlap its tip. This may work to our advantage, because the tip likely turns away in space and its velocity would suffer from an additional projection effect, which would not be easily quantified. As for determining the jet length, if the jet curved because of precession then we have indeed calculated a smaller jet length and underestimated its age. Similarly, if the angle of the jet is larger than 12 degrees, as assumed, then the de-projected velocity should be smaller and the jet older. It is possible that the time lag between CE ejection and jet be not so extreme, something that would help the interpretation of a post-CE jet as resulting from fall-back of material (Section §5).

As is the case for the other analysed PN, a final concern is that the structures were decelerated by ploughing up mass on their way. If the structures have been decelerated both their sizes and current velocities would be smaller than they should be. We ventured to guess that the jets would have been launched in a more evacuated environment since, as has been discovered by CE simulations (e.g., Sandquist et al. 1998 and Passy et al. 2012), the CE ejection is equatorial. As a result, it is likely only a small amount of mass would be swept up. In addition, if the jet material had been significantly decelerated, then the original launch velocities would be higher, something that would be hard to reconcile with typical accretors encountered in PN. We argue here, as we have done in Section §2.1 that any deceleration and mass loading should be within a factor of two and that this is supported by circumstantial

evidence of the similarity of these jet speeds with those found in the other known post-CE jet PN, FLEMING 1 (Section §6).

## 2.5 Conclusions from the data

For the jets in the PN Abell 63, Necklace and ETHOS 1 we can say that:

- (i) The jets predate the main nebula by  $\sim 5000$  yr.
- (ii) The jets have velocities of  $\sim 100 \text{ km s}^{-1}$ .
- (iii) For at least one central star (that of the Necklace PN), between  $0.03$  and  $0.45 M_{\odot}$  were accreted onto the companion (Miszalski et al. 2013).
- (iv) For at least one of our three jet pairs, the mass is  $\sim 10^{-3} M_{\odot}$ .

As explained in Section §2.1, Section §2.2 and Section §2.3, the uncertainties are large. However, we argue that the sequencing of jet and PN ejection is correct. We also argued that the jet speeds and ejected masses at the time of launch would not have been much higher than they are today. An additional cautionary note on the jet masses is that some gas may have recombined and was therefore not accounted for in our measurements.

The mass loss rate of the jets is calculated using the jet mass estimate for the Necklace PN and assuming that the jet was launched for the entire dynamical age minus the dynamical age of the nebula, equivalent to assuming that the jet was launched continually up to when the ejection of the CE took place. This results in a jet lifetime between  $\sim 4000$  and  $\sim 8000$  years for the Necklace nebula,  $\sim 6000$  yr for A 63 and  $\sim 5000$  yr for ETHOS 1. If the jet ejection timescales are lower, the jet mass-loss rates would be larger. We will further comment on this possibility in Section §3.

The PN NGC 6778 is different in that:

- (i) The jets formed after the main nebula by  $\sim 3000$  yr.
- (ii) There are two pairs of jets.
- (iii) The velocities of both pairs of jets are higher  $\sim 300 - 500 \text{ km s}^{-1}$ .
- (iv) The velocities of the two jet pairs are different.

From these characteristics, we can already deduce that the jets from NGC 6778 are a post-CE event. The jet launch points are either closer to the central accretor(s) or the accretor(s) are more massive than for the pre-CE jet objects. The jet mass loss rate is derived from the jet mass and a maximum jet lifetime of 1700 years.

It has to be emphasised that, although the formal errors could bring the age estimates of jets and ring to be much closer to one another, it is unlikely that the relative age estimates are completely unreliable. Looking at the data for the four objects in Table 1 and for the two additional objects which we discuss briefly in Section §6, we see a pattern, not only of relative ages, but also of jet speeds (slow for the pre-CE jets, faster for the post-CE jets). Although only improved measurements will refine this statement, it does appear that there are two distinct classes of CE jets.

Below we consider three physical mechanisms for the accretion and ejection of mass: ejection of mass by radiative pressure (section §3.1) and jet formation via an accretion disk formed at the time of Roche lobe (RL) overflow (section §3.2) or before RL overflow (section §3.3). In order to be consistent with the calculations in each model, we have adopted the following parameter ranges:

- Mass of the jets:  $M_{\text{jet}} \sim 10^{-3} M_{\odot}$ , this is based on the jet masses of Necklace PN and NGC 6778.
- Velocity of the jets:  $v \approx 100 \text{ km s}^{-1}$  or  $400 \text{ km s}^{-1}$ .

- Maximum duration of jet launching:  $4000 - 8000$  yr for pre-CE jets,  $\tau \sim 1700$  yr for post-CE ones.
- The mass-loss rate of the jets is  $1 - 3 \times 10^{-7}$  or  $8.8 \times 10^{-7} M_{\odot} \text{ yr}^{-1}$  for the pre and post-CE jets, respectively.
- Mass of the companion:  $M_{\text{sec}} \sim 0.3 M_{\odot}$ .
- Mass of the primary's core:  $M_{\text{core}} \sim 0.55 M_{\odot}$ .
- Mass of the primary's envelope:  $M_{\text{env}} \sim 0.45 M_{\odot}$ .

The mass assumptions are appropriate for a  $1.2 M_{\odot}$  main sequence star, which is the median mass of the PN population (Moe & De Marco 2006). Such stars leave behind a  $\sim 0.55 M_{\odot}$  core (Weidemann 2000; De Marco et al. 2011). At the time of interaction, the star is a giant and has a mass smaller than its main sequence mass. We therefore account for an envelope mass of  $0.45 M_{\odot}$ , so that our giant's total mass is  $1 M_{\odot}$ . The most represented stellar companion around white dwarfs has a spectral type M3.5V (Farihi et al. 2005) which translates in a mass of  $\sim 0.3 M_{\odot}$  (De Marco et al. 2013).

## 3 ACCRETION AND EJECTION MECHANISMS FOR JETS FROM COMMON ENVELOPE SYSTEMS

In our jet launching model, we assume that the accretion rate through the disk is  $\sim 10$  times the jet mass-loss rate derived in Section §2.5 (Sheikhnezami et al. 2012). Before we use these values of the accretion rate to derive the magnitude of the magnetic field (Section §4), we consider the likely accretion rates in a series of probable accretion scenarios. Although many assumptions are made to derive values of accretion rates, such estimates provide one additional consistency check, which helps to gauge the reliability of the overall jet launch scenarios.

### 3.1 Radiative Pressure

To calculate the radiative pressure exerted we use the brightest possible post-AGB star with  $L \approx 10^4 L_{\odot}$ . Hence the radiative force,  $\dot{p} = L/c$ , is  $10^{27}$  dyne. This is the largest possible force, exerted if the entire radiation field of the star were intercepted by jet matter and converted to kinetic energy with maximum efficiency.

The smallest jet force in our sample is obtained for the pre-CE jets by using  $M_{\text{jet}} = 10^{-3} M_{\odot}$  and velocity  $v = 100 \text{ km s}^{-1}$  (section §2.5) with an accretion timescale of 8000 years. This results in  $\dot{p}_{\text{jet}} \geq 8 \times 10^{25}$  dyne. A larger momentum limit can be obtained by using the fast jets of NGC 6778 (Table 1) with a mean jet velocity of  $460 \text{ km s}^{-1}$ :  $\dot{p}_{\text{jet}} \geq 2 \times 10^{27}$  dyne.

Comparing the lower limit range  $8 \times 10^{25} - 2 \times 10^{27}$  dyne to the upper limit of  $10^{27}$  dyne, it is easy to convince ourselves that radiation is unlikely to be responsible for the acceleration of these jets, not to mention that even if it were, there would be no explanation for the collimated nature of the outflows. We next turn our attention to accretion as a means to launch the jets.

### 3.2 The accretion rate at the time of Roche lobe overflow

The most logical moment to form an accretion disk in the life of a binary about to enter a CE interaction is at the time of RL overflow. To determine the mass accretion rate through the inner Lagrangian point we adopt, as a typical configuration, a  $1 M_{\odot}$  giant with a  $300 R_{\odot}$  radius, entering RL contact with a  $0.3 M_{\odot}$  companion at 3 AU. Such system may be close to reaching synchronisation at the time of RL overflow.

A formalism for the accretion rate through the inner Lagrangian point is given by Ritter (1988)<sup>1</sup>. They define the accretion rate as:

$$\dot{M} = \frac{2\pi}{\sqrt{e}} F(q) \frac{R_{L1}^3}{GM_1} \left( \frac{\mathcal{R}T_{\text{eff},1}}{\mu_{\text{ph},1}} \right)^{\frac{3}{2}} \rho_{\text{ph},1}, \quad (1)$$

where  $R_{L1}$  is the RL radius of the donor, in our case the primary giant,  $\mathcal{R}$  is the ideal gas constant,  $G$  is the gravitational constant,  $M_1$  is the mass of the primary,  $T_{\text{eff},1}$  the effective temperature of the primary,  $\mu_{\text{ph},1}$  is the mean molecular weight of the primary's atmosphere and  $\rho_{\text{ph},1}$  is the density at the photosphere.  $F(q)$  is defined as:

$$F(q) = (g(q) [g(q) - q - 1])^{-1/2} \left( \frac{R_L}{a} \right)^{-3} \quad (2)$$

with  $g(q) = q/x^3 + 1/(1-x)^3$  and where  $x$  is the distance of  $L_1$  to the secondary in units of  $a$ . The value for  $x$  can be calculated numerically based upon the orbital parameters of the system (Sepinsky et al. 2007, figure 4). The value of  $x$  is 0.40 or  $1.35 \times R_{L2}/a$ . We also used  $T_{\text{eff},1} \sim 3000$  K,  $\mu_{\text{ph},1} \sim 0.8$  (appropriate for a neutral cosmic mix), and  $\rho_{\text{ph},1} \sim 10^{-9}$  g cm<sup>-3</sup> (appropriate for our AGB star's atmosphere). Finally, from Eggleton (1983) the equation for the unit-less Roche radius of the primary is:

$$r_{L1} = \frac{R_{L1}}{a} = \frac{0.49q^{-\frac{2}{3}}}{0.6q^{-\frac{2}{3}} + \ln\left(1 + q^{-\frac{1}{3}}\right)} \quad (3)$$

where  $q = M_{\text{sec}}/M_{\text{prim}}$ ,  $R_{L1}$  is the RL radius for the primary, donor star and  $a$  is the separation between the two objects. In this way we found  $\dot{M} = 4 - 8 \times 10^{-4} M_{\odot} \text{ yr}^{-1}$ . We conclude that the RL overflow generates an accretion rate that may generate jets with a higher mass-loss rate and overall larger masses. This could either indicate that the pre-CE jets are launched before RL contact, or that the time over which they were launched is smaller, of the order of several decades, compared to the timescales we have adopted.

Finally, we remark that for an accretion rate of  $8 \times 10^{-4} M_{\odot} \text{ yr}^{-1}$  and an accreted mass of  $0.4 M_{\odot}$  (see Section §2.1), the accretion timescale would be 500 years. This timescale is lower by a factor of a few than the maximum ejection timescales listed in Table 1. As scenarios and data are refined, all these timescales need to be reconciled.

### 3.3 Wind Accretion

The issue of how long the system remains in RL contact before the onset of a CE is important, because the more of the envelope is transferred to the companion the easier it will be for the companion to unbind the remaining envelope during the CE phase (both because the envelope is lighter and because the companion is more massive). In Section 3.2 we have concluded that the phase may not

<sup>1</sup> Davis et al. (2013) also provide a similar derivation; however, there are inconsistencies between these two papers. The formulae we use follow Ritter (1988), but correct a mistake in the algebra where the exponent  $-3/2$  in their equation A8 should have been  $-3$ . Davis et al. (2013) have the correct exponent in their equation 9, but in the same equation they have multiplied by  $q$ , which is absent in the derivation of Ritter (1988). It should be noted, however, that the effect of the differences between the expressions used by Davis et al. (2013) and by Ritter (1988) was minimal.

be particularly short because we have assumed that the mass accretion that gives rise to the observed jets takes place due to RL overflow. Here we consider the possibility that the accretion takes place before RL overflow via accretion from the wind of the primary. If this took place it may release the constraint of needing much accretion to take place at the time of RL overflow.

The Bondi-Hoyle mass accretion approximation (BH; Bondi & Hoyle 1944) cannot be used to investigate accretion at separations of a few AU, or just outside the RL overflow separation. The BH capture radius,  $b = 2GM/(v_{\text{Kep}}^2 + v_{\text{wind}}^2)^{1/2}$ , where the Keplerian ( $v_{\text{Kep}}$ ) and wind ( $v_{\text{wind}}$ ) velocities are similar, is of the order of the orbital separation. In such case the BH approximation cannot be valid since the medium through which the accretor/companion is moving is all but homogeneous.

Unfortunately, there are no analytical accretion models for the region just beyond RL contact. However, a few simulations have explored this region, either through the simulation of both the primary and secondary (Mohamed & Podsiadlowski 2007, 2011; Kim & Taam 2012), or considering only one star (Huarte-Espinosa et al. 2012). Mohamed & Podsiadlowski (2007, 2011) propose an intermediate accretion mechanism that they call ‘‘wind RL overflow’’, where instead of the envelope of the primary filling the RL, its wind is channelled through the inner Lagrange point, allowing for an accretion rate that can be as high as half the mass-loss rate of the primary ( $10^{-6} - 10^{-4} M_{\odot} \text{ yr}^{-1}$ , for upper AGB stars) and much higher than the typical BH efficiency of a few percent. However, wind RL overflow may not always be applicable, as it requires that the velocity of the AGB wind at the RL radius be less than the escape velocity from the same location which will be sensitive to the details of the wind acceleration model.

Huarte-Espinosa et al. (2012) simulated disk formation around a mass in a box with uniform fluid. Their disk mass for simulation setups that represented orbital separations between 10 and 20 AU ranged between  $7 \times 10^{-6}$  and  $6.5 \times 10^{-7} M_{\odot}$ . Such disk masses would be on the low side to explain our jets masses. However, better measurements and models that cover a wider parameter space, such as a smaller orbital separation may find some agreement.

## 4 THE MAGNETIC FIELD

Once an accretion disk forms, we require a mechanism to cause the material in the disk to lose angular momentum and launch the jets. The mechanism for the angular momentum loss that allows material to accrete onto the central object is a matter of debate (see, e.g., Stone 1997; Vishniac & Diamond 1993; Gammie & Johnson 2005). Here we assume that the angular momentum transport is provided by the magnetic field that is also responsible for launching the jets. This in turn allows us to use the magnitude of the accretion rate to estimate the magnetic field strength.

Wardle (2007) derived an estimate of field strength required in order to accrete given the radius of the disk and the accretion rate (cf. section 2.1 of Blackman et al. 2001). The derivation considers the azimuthal component of the momentum equation for the system, and assumes that the azimuthal component of the disk's velocity can be approximated by its Keplerian velocity, given the disk is thin. Under such conditions, we have a minimum magnetic field strength (in Gauss) of:

$$B \approx 0.2 \dot{M}_{-7}^{1/2} r_{\text{AU}}^{-5/4} \left( \frac{M}{M_{\odot}} \right)^{1/4}, \quad (4)$$

where  $M$  is the mass of the accretor, where  $\dot{M}_{-7}$  is the mass accretion rate in units of  $10^{-7} M_{\odot} \text{ yr}^{-1}$  and  $r_{\text{AU}}$  is the disk radius, in AU, at which the field has that strength. This formalism applies locally, meaning that for a disk with an inner and an outer radii, one would derive a range of values of the magnetic field strengths. Below we apply this approximation to derive the magnitude of the magnetic field in our systems. We emphasise here that while the formalism above is a reasonable predictor of the needed magnetic field strengths, the accretion rates and disk sizes are not well constrained. However, as observationally-derived quantities become better known (likely from a larger sample, rather than better measurements) PN observations should put more stringent constraints on the CE interaction.

#### 4.1 The magnetic fields in systems where the jets predate the nebula

Huarte-Espinosa et al. (2012), modelling wind accretion onto a companion orbiting at 10, 15 and 20 AU from the primary, obtained accretion disk sizes of  $\sim 1$  AU. A similar estimate for the disk radius is obtained in the case of RL overflow. Using the tidal equations of Zahn (1989) and the radius evolution of stars in the mass range  $1 - 4 M_{\odot}$ , the maximum separation for a tidal capture is  $5 - 8$  AU, but for the more common lower mass stars it is closer to  $2 - 3$  AU (e.g., Villaver & Livio 2009; Mustill & Villaver 2012), which is also the distance at which our typical 300- $R_{\odot}$  giant will fill its RL. For a separation of 2.5 AU and a mass ratio of  $M_2/M_1 = 0.3$ , as adopted previously, we therefore expect the accretion disk radius to be smaller than the accretor's RL radius, or smaller than about 0.7 AU. Table 2 shows the required field strength using Equation (4) with a range of accretion rates appropriate for wind and RL overflow accretion which also encompass the values deduced from the jet mass-loss rates (Table 1) and for accretion disk radii of 0.5, 1 and 2 AU which encompass likely values of such disks. We emphasise that these disk radii are to be interpreted as distances from the accretor where disk material would be losing angular momentum at a rate dictated by the local magnetic field and at which point a certain fraction of that material, assumed to be 10%, would be launched vertically into a jet. Therefore the disk may extend to smaller and larger radii than the radius considered, but the magnetic field strength derived is for that location in the disk.

We finally note that the escape velocity from the gravitational field of accretors with masses between 0.3 and  $1 M_{\odot}$ , from a point located between 0.5 and 2 AU from the centre of the accreting secondary, are in the range  $16\text{-}60 \text{ km s}^{-1}$ . These are lower than the jet speeds of  $\sim 100 \text{ km s}^{-1}$  measured for systems where the jets predate the CE ejection. To obtain such larger jet velocities, we would need disk radii of 0.05-0.2 AU or  $10\text{-}45 R_{\odot}$ . So if we adopted a purely empirical approach, where we took a disk radius based on the jet speeds and an accretion rate of  $2 \times 10^{-6} M_{\odot} \text{ yr}^{-1}$  (or ten times the jet mass-loss rate from Table 1), we would derive magnetic field strengths of  $5 - 30$  G (see Table 2).

#### 4.2 The magnetic field in NGC 6778: an indirect measurement of a post-CE magnetic field

For the post CE PN NGC 6778 we know with reasonable certainty that the jets were launched after the CE dynamical infall phase. The two pairs of jets appear to be kinematically distinct so we also infer that they are not an optical illusion, part of the same kinematic

structure under specific illumination conditions (as is the case for M2-9; Livio & Soker 2001). It is however difficult to construct a physical scenario for the launching of these jets because the post CE orbital separation leaves but a small space within which to form a sufficiently massive accretion disk (but see Section §5).

However, on the assumption that these post-CE jets are indeed launched by a disk, we use their mass loss rate to infer a lower limit on the strength of the magnetic field necessary using Equation (4). Using the mass loss rate in the jets of  $8.8 \times 10^{-7} M_{\odot} \text{ yr}^{-1}$  (Table 1) and assuming, as we have done throughout this paper, that the accretion rate must be 10 times higher, and for a disk radius of 1 and  $10 R_{\odot}$ , we obtain a magnetic field of  $80 - 1400$  G (see Table 3). The orbital period of the binary today (Table 1), implies an orbital separation of approximately  $1 R_{\odot}$  for any plausible range of stellar masses. We include a larger disk radius in Table 3 to encompass the possibility that at the time of the jet launching either the orbital separation was larger or that the disk was circumbinary (see Section §5). We note that for an accretor in the mass range  $0.3 - 1.0 M_{\odot}$  and a launch point between 1 and  $10 R_{\odot}$ , the escape velocity ranges between  $110$  and  $620 \text{ km s}^{-1}$ , a range encompassing the deprojected velocities measured for the jets of NGC 6778 (Table 1).

We leave speculation of the actual scenario that gave rise to the post-CE twin jets to Section §5.

#### 4.3 The origin of the magnetic field

For the three systems where the jets predate the nebula, Gauss-sized magnetic fields are implied. These fields should thread the disk approximately vertically for the launching to happen according to commonly-adopted jet launching models (Blandford & Payne 1982). The magnetic field could originate in the envelope of the giant as it gets spun up by the tidally-infalling companion. The field would have to be dragged as the envelope material moves towards the companion. It is less likely that the magnetic field would originate in the companion itself, because of the relative old age of post-AGB binaries. One may also speculate that the field may be somehow self generated in the disk itself (for a discussion on different field configurations see Pudritz et al. 2007). Magnetic fields strengths on the surface of Miras have been measured and are consistent with a few Gauss. For example Amiri et al. (2012) measured a field strength of 3.5 G at 5.4 AU from the centre of the Mira star OH44.8-2.3.

For NGC 6778, whose launch model is so uncertain, it is paradoxically easier to hypothesise that the strong fields are created during the dynamical phase of the CE interaction, as detailed by Regos & Tout (1995) and Nordhaus et al. (2007). Nordhaus et al. (2007) modelled a CE dynamo in a  $3 M_{\odot}$  primary with secondaries in the mass range  $0.02 - 0.05 M_{\odot}$ . They find that the toroidal field,  $B_{\phi} \approx 1 - 2 \times 10^5$  G, while the poloidal component, responsible for the jet launching,  $B_p \approx 200 - 300$  G.

Regos & Tout (1995), provide an analytical formalism which we use here to derive the magnetic field components  $B_{\phi}$  and  $B_p$ . We start with the equation for the poloidal component of the magnetic field (Regos & Tout 1995, equation 2.14):

$$B_p = 10\gamma \left( \frac{3M_{\text{env}}}{R_{\text{env}}^3} \right)^{1/2} \left( \frac{LR_{\text{env}}}{\eta M_{\text{T}}} \right)^{1/3},$$

where the efficiency of the dynamo regeneration term is  $\gamma \sim 10^{-2}$ ,  $\eta = 3R_{\text{env}}/l_c \sim 30$ ,  $R_{\text{env}}$  is the radius of the base of the envelope,  $l_c$  is the mixing length parameter,  $L$  is the total energy generated

**Table 2.** Minimum field strengths required to launch jets in the systems where jets predate the main nebula

Mechanism	Approximate separation (AU)	Accretion rate ( $M_{\odot} \text{ yr}^{-1}$ )	Field strength for $r_{disk} = 0.1 \text{ AU}$ (G)	Field strength for $r_{disk} = 0.5 \text{ AU}$ (G)	Field strength for $r_{disk} = 1 \text{ AU}$ (G)	Field strength for $r_{disk} = 2 \text{ AU}$ (G)
Wind accretion	$\sim 3 - 5$	$10^{-6} - 10^{-5}$	8 – 26	1.1 – 3.5	0.5 – 1.5	0.2 – 0.5
RL overflow	$\sim 2 - 3$	$10^{-4} - 10^{-3}$	83 – 260	11 – 35	5 – 15	2 – 6

**Table 3.** Field strengths required to launch jets in NGC 6778

Accretion Rate ( $M_{\odot} \text{ yr}^{-1}$ )	Field strength for $r_{disk} = 1 \text{ R}_{\odot}$ (G)	Field strength for $r_{disk} = 10 \text{ R}_{\odot}$ (G)
$\sim 10^{-6}$	475 G	26 G
$\sim 10^{-5}$	1.6 kG	92 G
$\sim 10^{-4}$	4 kG	215 G

in the envelope, and  $M_T = M_{env} + M_R + M_W$ , where  $M_{env}$  is the mass of the envelope,  $M_R$  is the mass of the secondary (they “red” star), and  $M_W$  is the mass of the core (the future white dwarf). The total luminosity is  $L = L_{stars} + L_{orb}$ , where:

$$L_{stars} = \frac{1.869 \times 10^4 M_W^7 + 7.205 \times 10^6 M_W^9}{1 + 7.543 \times 10^2 M_W^5 + 1.803 \times 10^2 M_W^7},$$

(Regos & Tout 1995, equation 5.1) with  $L_{stars}$  and  $M_W$  in solar units. By combining their equations 4.6 and 4.9 to 4.11 and solving the resulting quadratic equation, we derive:

$$L_{orb} = \frac{L_{stars} (1 + \sqrt{1 + 4a})}{2a}, \quad (5)$$

with:

$$a = \frac{\eta M_T L_{stars}}{\Delta \Omega} \left( \frac{10}{M_{env} R_{env} \Omega_{orb}} \right)^2,$$

where  $\Delta \Omega = |\Omega_{orb} - \Omega_{env}|$  is the difference (or shear) between the angular velocity of the orbit ( $\Omega_{orb} = \sqrt{G(M_W + M_R)}/d^3$ , where  $d$  is the orbital separation), and that of the envelope. We read the value of the shear from figure 5 of Regos & Tout (1995). Finally, to determine  $B_{\phi}$ , we use their equation 2.4:  $B_{\phi} = B_p/\epsilon$ , with

$$\epsilon = \sqrt{\frac{0.01 \left( \frac{R_{env} L}{\eta M_T} \right)^{1/3}}{\Delta \Omega R_{env}}}.$$

Using a primary composed of an envelope with mass ranging between 0.5 and 2.5  $M_{\odot}$  and a core ranging between 0.5 and 1  $M_{\odot}$ , and a secondary with mass ranging between 0.5 and 1.5  $M_{\odot}$ , we found that  $B_{\phi} \approx 0.5 - 1 \times 10^4 \text{ G}$  and  $B_p \approx 100 - 500 \text{ G}$ . Therefore Regos & Tout (1995) and Nordhaus et al. (2007) agree on the magnitudes of the magnetic fields generated during a CE interaction. They both suggest that the field in post-CE primaries would be mostly toroidal, but that their poloidal component is still relatively strong and similar to what we have determined using our jet observations, for the larger of the disk radii considered (Table 3). What we have not considered here is that the magnetic field would likely be transported out with the ejection of the CE, so that its strength at the location of the remnant binary would decrease in time.

## 5 A SCENARIO FOR NGC 6778

Explaining the post-CE jet pairs observed in NGC 6778 is extremely difficult. At first sight, the two jets may indicate the for-

mation of two accretion disks, possibly due to the infall of material that was not fully ejected by the CE interaction (see, e.g., Akashi & Soker 2008). Such scenario may naturally explain the different jet velocities and even their morphologies. A simpler model whereby the jets are promoted by accretion of secondary star gas overflowing the RL and transferring to the primary via a disk may also be considered as was done by Soker & Livio (1994). This is a plausible scenario since in a binary with only  $1 \text{ R}_{\odot}$  separation, the secondary star, with a radius of 0.5-1  $\text{R}_{\odot}$  may indeed overflow its RL.

In both scenarios the limited space between the two stars may limit excessively the mass of the disk that can form. In the RL-overflow scenario of Soker & Livio (1994) it would be hard to explain the two jets with their distinct kinematics. A third scenario already considered by Kashi & Soker (2011) may be the formation of an accretion disk around both stars in the binary. However this would again not justify the two jet pairs. Additional scenarios may be constructed, for example one where the primary core spindown and strong magnetic fields expected after the CE ejection may form a jet in addition to one formed by a disk (Blackman et al. 2001). However such scenario rely on complex physical mechanisms which may or may not be at play in these stars.

A further constraint on any scenario is the time between the CE ejection and the post-CE jet ejection ( $\sim 3000 \text{ yr}$ ). Despite the difficulties mentioned above, we try here to determine whether a fallback disk would form within such a time frame. We here consider the infall of bound CE material and determine at what distance it would come to rest if we consider a simple ballistic trajectory and conservation of energy and angular momentum. By solving:

$$\begin{aligned} J_z &= m v_{\theta,h} h, \\ m v_{\theta,h} h &= m v_{\theta,disk} r_{disk}, \\ \frac{1}{2} v_{\theta,h}^2 - \frac{GM}{h} &= \frac{1}{2} v_{\theta,disk}^2 - \frac{GM}{r_{disk}} \end{aligned} \quad (6)$$

where  $J_z$  is the angular momentum vector perpendicular to the orbital plane,  $m$  is a mass element of in falling material,  $v_{\theta,h}$ ,  $v_{\theta,disk}$ ,  $h$  and  $r_{disk}$  are the orbital velocities and orbital radii of the material at altitude  $h$  above the compact binary and at the altitude at which the disk comes to rest;  $M$  is the mass of the central binary.

In order to put some numbers into the solution, we refer to the CE simulations of Passy et al. (2012) for our estimates of the angular momentum of the infalling envelope gas and its initial distance from the central binary. The  $z$  component of the total angular momentum of the system,  $J_z \approx 2.5 \times 10^{52} \text{ g cm}^2 \text{ s}^{-1}$ , was estimated by Passy et al. (2012) using a binary with  $M_1 = 0.88 M_{\odot}$ ,  $M_2 = 0.6 M_{\odot}$  and  $a = 83 \text{ R}_{\odot}$  (see their figure 8), where the angular momenta of the orbit and the envelope were considered. Of this, approximately 1/5 belongs to bound matter (Passy et al. 2012, see their figure 8). Bound material is distributed at  $h \sim 1 - 4.5 \times 10^3 \text{ R}_{\odot}$  (Passy et al. 2012, see their figure 19). If we divide the bound angular momentum by the mass of the bound envelope, using 95% of an envelope of 0.49  $M_{\odot}$ , we get the value of the specific angular momentum of the in-



falling material:  $v_{\theta,h}h \sim 5 \times 10^{18} \text{ cm s}^{-1}$ , which in turn gives  $v_{\theta,h} \approx 1.5 - 7.2 \times 10^4 \text{ cm s}^{-1}$ . Hence, using Equation (6), we calculate that the gas should come to rest at a distance from the binary centre of mass of approximately  $0.06 - 20 R_{\odot}$ . Hence, some of the fallback material will move closer to the centre of the binary than the orbital separation. Some of this material may have the correct angular momentum to form accretion disks around the two binary components, while some will be accreted directly onto the stellar surfaces or ejected from the system.

In order to determine the timescale of falling matter, we note that the gas follows half a Keplerian orbit with semi major axis  $a = (h + r_{\text{disk}})/2$ , so by symmetry, the time taken is half the orbital period, or:

$$t = \pi \sqrt{\frac{a^3}{GM}}.$$

The result of this is the time taken for the mass element to fall to the equilibrium position,  $t \sim 2 - 14 \text{ yr}$ . A more accurate ballistic calculation kindly carried out by J.-C. Passy using the results of his simulations (Passy et al. 2012), results in slightly longer timescales of  $8 - 50 \text{ yr}$ , because this calculation accounts for the fact that the bound material is still carrying some outward velocity.

Other physical mechanisms can be present that can slow down the infall: a fast wind from the central binary as well as radiation pressure. Using equation 6 from Soker (2001):

$$\frac{L/c}{\dot{M}_{\text{wind}} v_{\text{wind}}} = 10 \left( \frac{L}{5000 L_{\odot}} \right) \left( \frac{\dot{M}_{\text{wind}}}{10^{-8} M_{\odot} \text{ yr}^{-1}} \right)^{-1} \left( \frac{v_{\text{wind}}}{1000 \text{ km s}^{-1}} \right)^{-1},$$

where  $L$  is the luminosity of the giant's core,  $\dot{M}_{\text{wind}}$  and  $v_{\text{wind}}$  are the mass-loss rate and velocity of the wind, respectively and  $c$  is the speed of light. Here we have rescaled his values to those of an intermediate mass central stars ( $0.58 M_{\odot}$ ) transiting towards the white dwarf cooling track. The ram pressure of the wind is therefore a tenth of the radiation pressure and will not play a significant role in slowing down the infall.

To estimate the radiation pressure, we can again use Soker (2001). Using their equations 1, 2, 4 and 5, we can compute the ratio of the gravitational force to the radiative force, given by:

$$\frac{f_g}{f_r} = \frac{\frac{GMm}{r^2}}{\frac{L}{c} \beta (1 - e^{-\tau})} \quad (7)$$

where  $m$  is a mass element at distance  $r$  from the central binary with total mass  $M$  and luminosity  $L$ , subtending a solid angle  $\Omega$  such that  $\beta = \Omega/2\pi$  and where  $\tau$  is the optical depth of the mass element. The optical depth of the infalling envelope is not easy to determine at present. However, even assuming that the material is optically thick, and that it subtends the entire solid angle, the gravitational force dominates by more than four orders of magnitude. Thus we deduce that radiation would not have much of a retarding effect on the infalling material. Lacking a way to retard the formation of a fall-back disk, we must conclude that such a short return timescale is at odds with the thousand-year-timescale indicated by the kinematics (unless the kinematic age of the jets were lower, or that of the disk higher).

## 6 COMPARISON WITH CE PN FLEMING 1 AND NGC 6337

There are two additional PN with jets known to harbour post-CE binaries: Fleming 1 and NGC 6337. We have not included them directly in our study because of the lack of nebular mass information.

Below we review those characteristics which can be found in the literature and compare them to those of the 4 cases studied here.

Fleming 1 has jets that pre-date the nebula (Lopez et al. 1993; Palmer et al. 1996), as is the case for A 63, ETHOS 1 and the Necklace nebula. Fleming 1, with a 5000 year old main nebula and 16000 year old jets has the highest time interval between jet and CE formation. Its orbital period today is 1.19 days, similar to the Necklace nebula. Its flat jet caps are more similar to those of A 63. This nebula is thought to harbour a double degenerate star (Boffin et al. 2012). The deprojected fastest velocity of the knotty jets of Fleming 1 is  $\sim 100 \text{ km s}^{-1}$ , assuming, as Boffin et al. (2012) have done, an inclination of 45 deg to the line of sight. This speed is in line with those of the other pre-CE jets.

NGC 6337, has post-CE jets as is the case for NGC 6778. The post-CE jets of NGC 6337 have many similarities with those of NGC 6778. Using the distance of Frew (2008) of  $0.86 \pm 0.20 \text{ kpc}$  (instead of the distance of  $1.3 \text{ kpc}$  of García-Díaz et al. (2009)), the ages of the nebula and jets are  $\sim 8000$  and  $\sim 1000$  years, respectively, a 7000 year delay between the CE and the jet ejection (cf. with almost 3000 years for NGC 6778). The jet velocity is  $\sim 200 \text{ km s}^{-1}$ , smaller than the velocity of the jets of NGC 6778 ( $270$  and  $460 \text{ km s}^{-1}$ , for each of the two pairs), but larger than all the pre-CE jet speeds. The jets in NGC 6337 are bent as is one of the jet pairs in NGC 6778. The binary inside NGC 6337 has an orbital period of 0.17 days, similar to the very short period of the binary inside NGC 6778 (0.15 days).

Hillwig et al. (2010) modelled the lightcurve of the central binary in NGC 6337 and, by assuming a central star mass of  $0.6 M_{\odot}$ , derived a companion mass of  $0.2 M_{\odot}$  (quoting the hotter of the two models presented, but the differences are not large). This results in a situation where the companion, with a radius of  $0.34 M_{\odot}$ , is close to filling its RL (the inner Lagrangian point is only  $0.56 R_{\odot}$  away from the centre of the secondary). While we have considered a model where the disk is formed by re-accretion of nebular material, we must wonder whether the coincidence of both binaries with post-CE jets being so close to RL overflow may not be telling us that the jet is actually due to accretion of secondary material onto the primary as proposed by Soker & Livio (1994). It is possible that in this case there differences in composition between the bulk of the nebula and the jet may be observed, since the jet may come from the unprocessed envelope of the main sequence secondary, rather than processed AGB envelope gas. Of course, this would be the case only if the envelope of the secondary were not highly contaminated by AGB envelope material accreted during the CE phase.

## 7 CONCLUSION AND DISCUSSION

We have analysed the jets and nebulae of four post-CE PN, starting with their masses and kinematics. Three of the PN, the Necklace, Abell 63 and ETHOS 1, have jets that predate the main nebula by a few thousand years. They may have arisen when an accretion disk formed around the companion at the time of RL overflow, although that may lead to accretion rates higher than needed to explain the observed jets. Alternatively the pre-CE jets may have formed before RL contact, from wind accretion, in which case accretion rates could be lower. The latter hypothesis is also more in line with the relatively long timescales of jet formation before the CE infall phase. Further studies of systems like this could enable their use as constraints on the pre-CE phase which is at the moment ill constrained.

The fourth PN, NGC 6778, has jets that lagged the main neb-

ula by about 3000 years. The two pairs of jets with different velocities, both higher than the jet velocities in the pre-CE jets, are difficult to explain by any scenario. Appealing to RL overflow of the companion after the CE ejection makes sense in view of the very small orbital separation of today's binary. However, the two pairs of jets are then difficult to explain. A scenario where fallback of envelope material forms one or two accretion disks around the binary or its components meets with difficulties both due to the need to delay the disk formation and the fact that the orbital separation is small enough that forming two disks would be difficult. Despite these difficulties it is clear that post-CE jets (of which there is at least another one in the PN NGC 6337) will be useful in constraining future simulations of the CE interaction.

Independently of the scenario that formed the accretion disks, we have derived the strength of the magnetic field that launches the jets using the assumption that it removes angular momentum at the rate needed for accretion of material and launches the jets according to the mechanism of Blandford & Payne (1982). If so, the magnetic field strengths are of a few to ten Gauss, for pre-CE jets and hundreds to a few kilo-Gauss in the case of post-CE jets. While it is unclear how to bring Gauss-strength fields to the proximity of the companion in a pre-CE binary, the strength of the post-CE fields is in line with the independent theoretical predictions of post-CE fields by Regos & Tout (1995) and Nordhaus et al. (2007).

Finally we remark that the jet masses and kinematics can provide us with the indication of how much envelope has been ejected before the CE via the jets, and how much has accreted to the companion. Both these phenomena will facilitate the envelope ejection, something that could explain the lack of a full CE ejection witnessed in the simulations of (Passy et al. 2012). Frew (2008) found that all CE PN have low ionised masses compared to the masses of other PN. This observation could be in line with the hypothesis of a decreased envelope mass.

Accretion onto the companion is supported by the observation of carbon-rich material on the secondary star in the post-CE central binary of the Necklace nebula (Miszalski et al. 2013). Accretion onto the companion during the dynamical infall phase was excluded by the theoretical work of Ricker & Taam (2008, 2012), implying that the accretion must have happened before the CE dynamical phase, likely during the preceding RL overflow of the giant.

## ACKNOWLEDGMENTS

We are thankful to Martin Guerrero and Romano Corradi for sharing their observations and deriving for us jet masses. We are also indebted with David Frew for providing us with a homogeneous set of distances to these PN, which may have improved the comparison between them. Jean-Claude Passy is thanked for calculating the ballistic trajectories of his common envelope simulations and confirming the analytical estimates of the fallback disks. Overall we are grateful for Noam Soker's extensive comments and criticisms. We are thankful to Jan Staff for sharing his theoretical knowledge of jets. Finally, we thank an anonymous referee for comments which allowed us to improve the paper. OD acknowledges Australian Research Council Discovery grant DP120103337 and Future Fellowship grant FT120100452; MJW acknowledges Discovery grant DP120101792.

## REFERENCES

- Abell G. O., 1966, *ApJ*, 144, 259  
 Acker A., 1992, in *Astronomy from Large Databases, II.*, Vol. 43, p. 163  
 Afşar M., Ibanoglu C., 2008, *MNRAS*, 391, 802  
 Akashi M., Soker N., 2008, *NewA*, 13, 157  
 Amiri N., Vlemmings W. H. T., Kemball A. J., van Langevelde H. J., 2012, *A&A*, 538, A136  
 Blackman E. G., 2009, in *Proceedings of the International Astronomical Union*, Vol. 259, pp. 35–46  
 Blackman E. G., Frank A., Welch C., 2001, *The Astrophysical Journal*, 546, 288  
 Blandford R. D., Payne D. G., 1982, *MNRAS*, 199, 883  
 Boffin H. M. J., Miszalski B., Rauch T., Jones D., Corradi R. L. M., Napiwotzki R., Day-Jones A. C., Köppen J., 2012, *Science*, 338, 773  
 Bond H. E., 2000, in *Asymmetrical Planetary Nebulae II: From Origins to Microstructures*, ASP Conference Series, Vol. 199, Vol. 199, p. 115  
 Bond H. E., Liller W., Mannery E. J., 1978, *ApJ*, 223, 252  
 Bondi H., Hoyle F., 1944, *MNRAS*, 104, 273  
 Corradi R. L. M. et al., 2011, *MNRAS*, 410, 1349  
 Davis P. J., Siess L., Deschamps R., 2013, *ArXiv e-prints*  
 De Marco O., Farihi J., Nordhaus J., 2009, *Journal of Physics Conference Series*, 172, 012031  
 De Marco O., Passy J.-C., Frew D. J., Moe M., Jacoby G. H., 2013, *MNRAS*, 428, 2118  
 De Marco O., Passy J.-C., Moe M., Herwig F., Mac Low M.-M., Paxton B., 2011, *MNRAS*, 411, 2277  
 Eggleton P. P., 1983, *ApJ*, 268, 368  
 Farihi J., Becklin E. E., Zuckerman B., 2005, *ApJS*, 161, 394  
 Frew D. J., 2008, PhD, Macquarie University, Sydney, Australia  
 Frew D. J., Parker Q. A., 2010, *PASA*, 27, 129  
 Gammie C. F., Johnson B. M., 2005, in *Chondrites and the Protoplanetary Disk*, Vol. 341, p. 145  
 García-Díaz M. T., Clark D. M., López J. A., Steffen W., Richer M. G., 2009, *ApJ*, 699, 1633  
 Geier S., Napiwotzki R., Heber U., Nelemans G., 2011, *A&A*, 528, L16  
 Guerrero M. A., Miranda L. F., 2012, *A&A*, 539, A47  
 Hambly N., Read M., Mann R., Sutorius E., Bond I., MacGillivray H., Williams P., Lawrence A., 2004, in *Astronomical Data Analysis Software and Systems (ADASS) XIII*, Proceedings of the conference held 12-15 October, 2003 in Strasbourg, France. Edited by Francois Ochsenbein, Mark G. Allen and Daniel Egret. ASP Conference Proceedings, Vol. 314. San Francisco: Astronomical Society of the Pacific, 2004., Vol. 314, p. 137  
 Hillwig T. C., Bond H. E., Afşar M., De Marco O., 2010, *AJ*, 140, 319  
 Huarte-Espinosa M., Carroll-Nellenback J., Nordhaus J., Frank A., Blackman E. G., 2012, *ArXiv e-prints*, 12  
 Ivanova N. et al., 2013, *A&ARv*, 21, 59  
 Kashi A., Soker N., 2011, *MNRAS*, 417, 1466  
 Kim H., Taam R. E., 2012, *ApJ*, 759, 59  
 Livio M., Soker N., 2001, *ApJ*, 552, 685  
 Lopez J. A., Meaburn J., Palmer J. W., 1993, *ApJ*, 415, L135  
 Maestro V., Guerrero M. A., Miranda L. F., 2004, in *ASP Conference Proceedings*, Vol. 313, Vol. 313, p. 127  
 Miszalski B., Acker A., Parker Q. A., Moffat A. F. J., 2009, *A&A*, 505, 249  
 Miszalski B., Acker A., Parker Q. A., Moffat A. F. J., 2009, *A&A*,

- 505, 249
- Miszalski B., Boffin H. M. J., Corradi R. L. M., 2013, *MNRAS*, 428, L39
- Miszalski B., Corradi R. L. M., Boffin H. M. J., Jones D., Sabin L., Santander-García M., Rodríguez-Gil P., Rubio-Díez M. M., 2011a, *MNRAS*, 413, 1264
- Miszalski B., Jones D., Rodríguez-Gil P., Boffin H. M. J., Corradi R. L. M., Santander-García M., 2011b, *A&A*, 531, 5
- Mitchell D. L., Pollacco D., O'Brien T. J., Bryce M., López J. A., Meaburn J., Vaytet N. M. H., 2007, *MNRAS*, 374, 1404
- Moe M., De Marco O., 2006, *ApJ*, 650, 916
- Mohamed S., Podsiadlowski P., 2007, in *Asymmetrical Planetary Nebulae IV*, p. 78
- Mohamed S., Podsiadlowski P., 2011, in *Why Galaxies Care about AGB Stars II: Shining Examples and Common Inhabitants*, Vol. 445, p. 355
- Mustill A. J., Villaver E., 2012, *ApJ*, 761, 121
- Nordhaus J., Blackman E. G., Frank A., 2007, *MNRAS*, 376, 599
- Paczynski B., 1976, in *IAU Symposium*, Vol. 73, *Structure and Evolution of Close Binary Systems*, Eggleton P., Mitton S., Whelan J., eds., p. 75
- Palmer J. W., Lopez J. A., Meaburn J., Lloyd H. M., 1996, *A&A*, 307, 225
- Parker Q. A. et al., 2006, *MNRAS*, 373, 79
- Passy J.-C. et al., 2012, *ApJ*, 744, 52
- Passy J.-C. et al., 2012, *ApJ*, 744, 52
- Pollacco D. L., Bell S. A., 1993, *MNRAS*, 262, 377
- Pudritz R. E., Ouyed R., Fendt C., Brandenburg A., 2007, *Protostars and Planets V*, 277
- Regos E., Tout C. A., 1995, *MNRAS*, 273, 146
- Ricker P. M., Taam R. E., 2008, *ApJ*, 672, L41
- Ricker P. M., Taam R. E., 2012, *ApJ*, 746, 74
- Ritter H., 1988, *A&A*, 202, 93
- Sandquist E. L., Taam R. E., Chen X., Bodenheimer P., Burkert A., 1998, *ApJ*, 500, 909
- Sepinsky J. F., Willems B., Kalogera V., 2007, *ApJ*, 660, 1624
- Sheikhnezami S., Fendt C., Porth O., Vaidya B., Ghanbari J., 2012, *ApJ*, 757, 65
- Soker N., 1997, *ApJS*, 112, 487
- Soker N., 2001, *MNRAS*, 328, 1081
- Soker N., Livio M., 1994, *ApJ*, 421, 219
- Stone J. M., 1997, in *American Physical Society, APS/AAPT Joint Meeting*
- Villaver E., Livio M., 2009, *ApJ*, 705, L81
- Vishniac E. T., Diamond P., 1993, *Advanced Series in Astrophysics and Cosmology*, 9, 41
- Wardle M., 2007, *Ap&SS*, 311, 35
- Weidemann V., 2000, *A&A*, 363, 647